How to cite: *Angew. Chem. Int. Ed.* **2025**, e202503626
doi.org/10.1002/anie.202503626

H_2O_2 Electrosynthesis | Hot Paper

Tuning Local Proton Concentration and *OOH Intermediate Generation for Efficient Acidic H_2O_2 Electrosynthesis at Ampere-Level Current Density

*Genwang Zhu, Shuaijie Zhao, Yueling Yu, Xinfei Fan, Kaiyuan Liu, Xie Quan, and Yanming Liu**

Abstract: Electrocatalytic oxygen reduction is a sustainable method for on-site H_2O_2 synthesis. The H_2O_2 in acidic media has wide downstream applications, but acidic H_2O_2 electrosynthesis suffers from poor efficiency due to high proton concentration and unfavourable *OOH (key intermediate) generation. Herein, acidic H_2O_2 electrosynthesis was enhanced by regulating local proton availability and *OOH generation via fluorine-doped on inner and outer walls of carbon nanotubes (F-CNTs). It was efficient and stable for H_2O_2 electrosynthesis with Faradaic efficiency of 95.6% and H_2O_2 yield of 606.6 mg cm^{-2} h^{-1} at 1.0 A cm^{-2} and 0.05 M H_2SO_4, outperforming the state-of-the-art electrocatalysts. The F-doping regulated the electronic structure of CNTs with elevated p-band center, and F-doping on its inner and outer walls also enhanced nanoconfinement effect and superhydrophobicity, respectively. As a result, a local alkaline microenvironment was created on F-CNTs surface during acidic H_2O_2 electrosynthesis. The energy barrier for *OOH generation was significantly reduced and oxygen mass transfer was boosted. Their synergistic effects promoted acidic H_2O_2 electrosynthesis. This work provides new insights into the mechanism for regulating H_2O_2 electrosynthesis.

Introduction

Hydrogen peroxide (H_2O_2) is one of the most important chemicals. The global demand for H_2O_2 has been increasing annually. It is anticipated that the global market size for H_2O_2 could reach $620 million by the year 2026.[1,2] At present, over 95% of H_2O_2 production relies on energy-intensive anthraquinone process, which produces organic wastes and has the risk of explosion during H_2O_2 transport.[3,4] Electrocatalytic two-electron oxygen reduction reaction ($2e^-$-ORR) provides an energy-efficient and green alternative method for on-site H_2O_2 production.[5,6] The H_2O_2 electrosynthesis under alkaline condition is usually more efficient than that under acidic condition. Due to the strong oxidation capability of acidic H_2O_2 solution, it has many application scenarios such as drug synthesis, disinfection, and wastewater treatment.[7–10] Therefore, efficient H_2O_2 electrosynthesis under acidic condition is an urgent demand.[7,10,11]

H_2O_2 electrosynthesis proceeds via oxygen reduction to *OOH ($*O_2 + H^+ + e^- \rightarrow$ *OOH, acid) and *OOH reduction ($*OOH + H^+ + e^- \rightarrow H_2O_2 + *$). Both *OOH generation and local pH are important for H_2O_2 electrosynthesis. The generation of *OOH with appropriate binding energy can enhance H_2O_2 production activity and selectivity, and suitable local pH is favorable for improving H_2O_2 selectivity. At acid solution, the excess H^+ around electrode interface can lead to H_2O_2 reduction or hydrogen evolution,[12,13] which decrease H_2O_2 selectivity, especially at industrial-relevant currents. There are only a few known electrocatalysts, including single atom catalysts, metal-based compounds, and carbon materials, demonstrated to be selective and stable for acidic H_2O_2 electrosynthesis.[14–17] Despite the progresses have been made, acidic H_2O_2 electrosynthesis still has low selectivity at industrial-relevant currents. Without the addition of alkali metal ions, simultaneous optimization of *OOH generation and local pH to enhance acidic H_2O_2 electrosynthesis remains a great challenge.

Carbon nanotubes (CNTs) feature well-defined internal cavity structure and tunable electronic property, which exhibit attractive activity and stability for alkaline H_2O_2 electrosynthesis.[18–22] Unfortunately, their performance in acid is unsatisfied.[23,24] By doping with highly electronegative fluorine atoms, the electronic structure of CNTs can be tuned, which is expected to optimize the reaction microenvironment and binding energy for *OOH.[25–27] The fluorine doped on CNTs inner walls (F-in-CNTs) can enhance the nanoconfinement effect of CNTs, thereby improving the reaction efficiency for H_2O_2 electrosynthesis. The fluorine doped on the outer surface of CNTs (F-out-CNTs) can create high hydrophobicity, which is conducive to oxygen reduction. It also avoids the cover of catalytic sites by hydrophobicity modification with polymers. However, regulating *OOH generation and local pH for acidic H_2O_2 electrosynthesis have been

[*] G. Zhu, S. Zhao, Y. Yu, K. Liu, Prof. Dr. X. Quan, Prof. Dr. Y. Liu
Key Laboratory of Industrial Ecology and Environmental Engineering (Ministry of Education, China), School of Environmental Science and Technology, Dalian University of Technology, Dalian116024, China
E-mail: liuyanm@dlut.edu.cn

Prof. Dr. X. Fan
College of Environmental Science and Engineering, Dalian Maritime University, Dalian116024, China

Additional supporting information can be found online in the Supporting Information section

rarely reported on CNTs. The mechanism for enhancing H_2O_2 electrosynthesis in acid remains insufficiently understood.

In this work, F-CNTs with F doped on the inner and outer surfaces were developed for regulating *OOH generation and local pH for acidic H_2O_2 electrosynthesis. Theoretical calculations and experimental results showed that both electronic structure and interface microenvironment were regulated by F-doping, resulting in superior performance for H_2O_2 electrosynthesis with Faradaic efficiency of 95.6% at 1.0 A cm^{-2} and 0.05 M H_2SO_4, outperforming the state-of-the-art electrocatalysts.

Results and Discussion

Synthesis and Characterization of F-CNTs

Fluorine atoms doped into carbon materials can alter their electronic structures. Here the function of fluorine atoms for catalysis was investigated by density functional theory (DFT) calculation. Considering the differences between doping in the inner and outer walls of CNTs as well as the nanoconfinement effect, the models of F-doped graphene (F-G), F-out-CNTs and F-in-CNTs were constructed to reveal the influence of fluorine atoms on carbon sites (Figure S1). The catalytic activity and adsorption energy of intermediates is closely correlated with p-band center (ε_p) of active sites.[28–30] Here the ε_p of carbon sites is shifted from −5.68 eV for CNTs to −4.79 eV for F-out-CNTs, which is further upshifted to −3.76 eV for F-in-CNTs (Figure 1a). It implies that F-doping regulates the electronic structure of F-CNTs, which can improve its electrocatalytic activity with suitable intermediate adsorption energy, and the improvement on F-in-CNTs is more significant. The ε_p of F-G (−4.97 eV) also shifts to high energy as comparison with G (−5.77 eV, Figure 1b), but its increment is lower than those of F-CNTs, suggesting that F-CNTs may be superior to F-G for H_2O_2 electrosynthesis. The nanoconfinement effect may play important roles (Figure 1c).

The F_x-CNTs (x represents F content) were prepared by pyrolyzing the mixture of polytetrafluoroethylene (PTFE) and CNTs (Figure S2). The PTFE and CNTs were mixed and ultrasonically treated until a uniform ink formed. During this process, PTFE was embedded into CNTs (Figure S3). The mixture was dried before pyrolyzing. Compared with the uniform lattice distances (0.345–0.348 nm) of CNTs (Figure 1d), the lattice distance of F_{10}-CNTs at some position is increased to 0.404 nm (Figure 1e). Because of the high electronegativity of F atom, it has a great influence on the electron cloud of neighboring carbon atoms, resulting in the change of the lattice spacing of CNTs (Figure S4). The XPS spectrum shows that F_{10}-CNTs possess an obvious F1s peak at 688.1 eV (Figure S5). Its C1s spectrum could be deconvolved into four peaks with binding energies at 291.3, 286.4, 285.1, and 284.8 eV, which are attributed to CF_3, CF_2, C─CF and C─C bonds, respectively. In its F1s XPS spectrum, the peaks with binding energy at 685.2, 687.2, and 693.9 eV could be assigned to semi-ionic C─CF, covalent CF_2 and covalent CF_3 (Figure 1f), indicating that F atoms have been successfully doped into the carbon skeleton and mainly existed in the form of CF_2.[27,31] The XPS depth-profiling analysis of F_{10}-CNTs reveals that its F content gradually decreases from 1.50 to 0.93 at% with the increase of etching depth at 0–15 nm (Figure 1g and S6). As the diameters of CNTs are 20–30 nm, F atoms have been doped into the inner and outer walls of CNTs with CF_2 as main species. Additionally, its BET surface area (92.5 m^2 g^{-1}) is increased in comparison with CNTs (64.43 m^2 g^{-1}), and the mean desorption pore size increases from 17.9 to 24.9 nm (Figure S7). X-ray diffraction (XRD) pattern of F_{10}-CNTs shows a graphite (002) peak at 26.5°. Compared with CNTs, its peak intensity and full width at half maximum decrease significantly (Figure S8). Raman spectra reveal that the intensity ratio of D and G band (I_D/I_G) is 0.48 for F_{10}-CNTs, higher than 0.27 for CNTs (Figure 1h). These results indicate that the doped F atoms can change the structure of CNTs, which may be favorable for H_2O_2 electrosynthesis.

Performance for H_2O_2 Electrosynthesis

The 2e⁻-ORR performance was tested by rotating ring-disk electrode (RRDE) in O_2-saturated 0.05 M H_2SO_4 (1600 rpm, Figure S9). F_{10}-CNTs have more positive onset potential and higher H_2O_2 selectivity than CNTs, indicating that F-doping is favorable for 2e⁻-ORR. To explore the impact of F-doping on H_2O_2 electrosynthesis, F_x-CNTs (x = 0, 4, 6, 8, 10, and 12) were prepared by changing the PTFE ratios in precursors. H_2O_2 electrosynthesis was conducted on them in a double-chamber flow cell with the counter electrode separated by Nafion 117 membrane (Figure S10). The catalyst was coated on carbon paper (2 cm × 2 cm) with a catalyst loading of 0.5 mg cm^{-2} (more details in Supporting Information). Figure 2a shows the Faradaic efficiencies for H_2O_2 production (FEs_{H2O2}) on F_x-CNTs are significantly enhanced as compared with CNTs (0.05 M H_2SO_4, 100–500 mA cm^{-2}), especially at higher current density. With the increase of fluorine content, both FEs_{H2O2} and H_2O_2 yields of F_x-CNTs are increased, and reach the maximum at F_8-CNTs and F_{10}-CNTs (Figure S11). Besides, F_{10}-CNTs exhibit more positive potential than CNTs and other F_x-CNTs under the same current density (Figure S12), which is −1.27 V (versus RHE) at 500 mA cm^{-2}. At 100–1000 mA cm^{-2}, FEs_{H2O2} of F_{10}-CNTs are 99.2%–95.6%, and its FE_{H2O2} almost keeps unchanged even if the current density is increased to 1000 mA cm^{-2} (Figure 2a,b). The corresponding H_2O_2 yields are 351.5–606.6 mg cm^{-2} h^{-1} at 600–1000 mA cm^{-2}. Interestingly, F_{10}-CNTs outperform the state-of-the-art electrocatalysts in terms of FE_{H2O2} and H_2O_2 yield under acidic conditions (Figure 2c and Table S1).

The physical and electrochemical properties of F_x-CNTs were studied to get insight into their different performance for H_2O_2 electrosynthesis. The F content of F_x-CNTs increases from 0.38 at% (F_4-CNTs) to 2.21 at% (F_{12}-CNTs) with the increase of PTFE ratio (Figure S13 and Table S2). The morphology of different F_x-CNTs have negligible difference (Figure S14). The I_D/I_G ratio is gradually increased and the intensity of graphite diffraction peak is decreased when F content is increased (Figures S15 and S16). F_x-CNTs have high hydrophobicity with water contact angles of 137.2°–140.4°

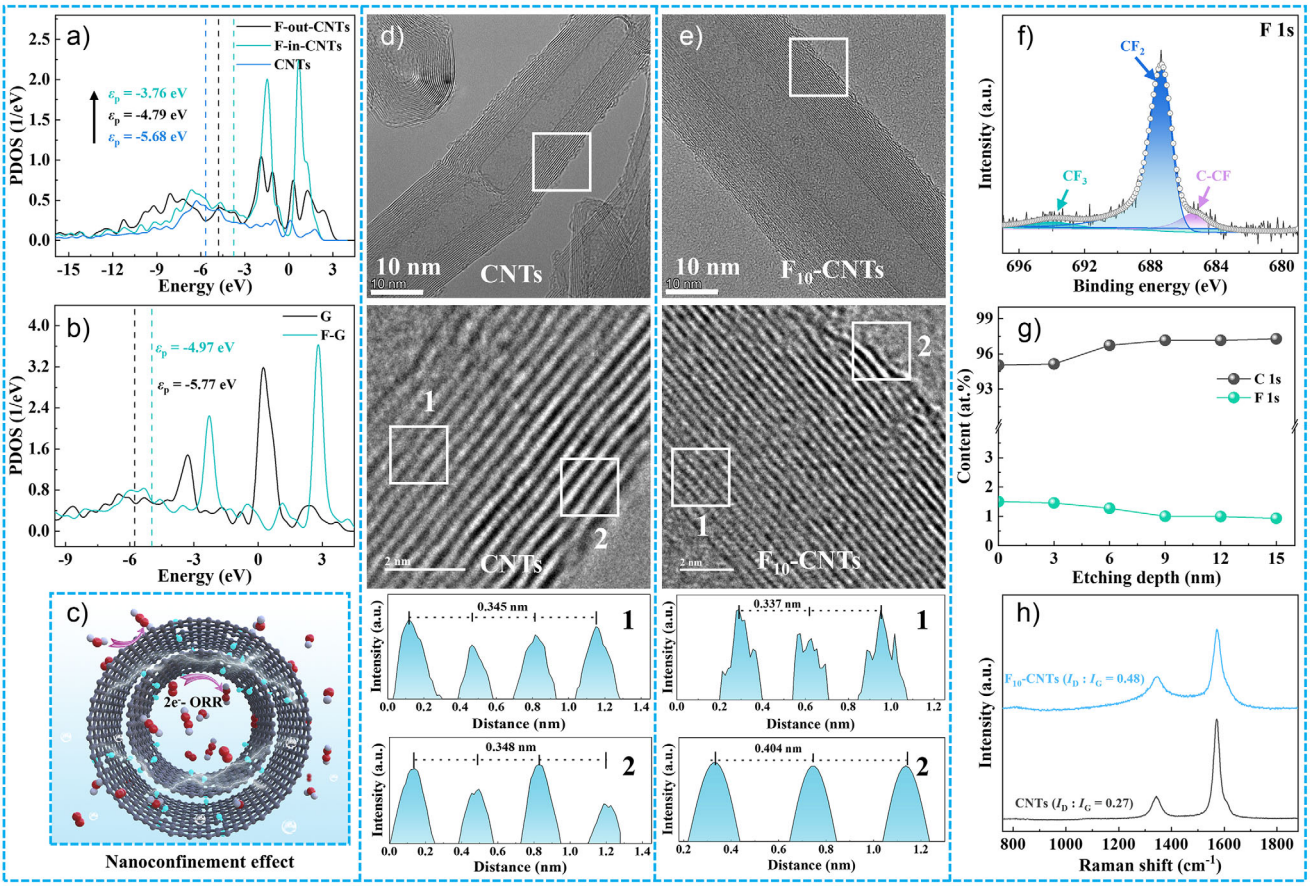

Figure 1. a) Projected density of states (PDOS) of F-in-CNTs, F-out-CNTs and CNTs. b) PDOS of G and F-G. c) Schematic diagram of nanoconfinement effect in F-CNTs. TEM images and interlayer distances of d) CNTs and e) F_{10}-CNTs. f) F1s XPS spectrum of F_{10}-CNTs. g) The contents of F, C and O from XPS depth-profiling analysis of F_{10}-CNTs (diameters: 20–30 nm). h) Raman spectra of CNTs and F_{10}-CNTs.

(Figures 2d and S17). As expected, their water contact angles are much higher than that of CNTs (24.6°), and they exhibit insignificant changes after H_2O_2 electrosynthesis. Their Tafel slopes are decreased with the increase of F content and reach the value of 44.4 mV dec^{-1} on F_{10}-CNTs (Figure 2e), implying its faster kinetics for 2e$^-$-ORR. The oxygen diffusion layer thickness is calculated based on the impedance data (Figures 2f and S18).[13] F_{10}-CNTs have lower diffusion layer thickness (2.9 μm) than others (3.3–6.1 μm), which enables its good oxygen mass transfer. These results indicate that F-doping improves the hydrophobicity, accelerates oxygen mass transfer, and reaction kinetics for H_2O_2 electrosynthesis on F_{10}-CNTs. The excessive F-doping on F_{12}-CNTs may result in its unsuitable electronic structure for the adsorption of intermediates/oxygen, and thereby reducing its H_2O_2 selectivity (Figure S9).

Reaction Mechanism for H_2O_2 Electrosynthesis

To explore the contribution of hydrophobicity for H_2O_2 electrosynthesis, hydrophobic CNTs was obtained by PTFE modification (CNTs@PTFE) and its performance for H_2O_2 electrosynthesis was compared with F_{10}-CNTs (Figure 3a). The CNTs@PTFE is selective for H_2O_2 electrosynthesis with FE_{H2O2} of 99.3% at current density ≤200 mA cm^{-2} and 0.05 M H_2SO_4, but its FEs_{H2O2} are decreased to 77.1%–44.9% at 300–500 mA cm^{-2}. Notably, the FEs_{H2O2} of CNTs@PTFE are significantly increased in comparison with CNTs (≥200 mA cm^{-2}, FE_{H2O2} <24.1%). However, both FEs_{H2O2} and H_2O_2 yields of CNTs@PTFE are still much lower than those of F_{10}-CNTs at 300–500 mA cm^{-2} (Figure S19). The water contact angle of CNTs@PTFE (139.4°) is similar to that of F_{10}-CNTs (Figure 3b). Therefore, hydrophobicity modification improves the FE_{H2O2} of CNTs to some extent, but it is not the dominant factor responsible for the superior performance of F_{10}-CNTs for H_2O_2 electrosynthesis.

To get insight into the superior performance of F_{10}-CNTs for H_2O_2 electrosynthesis, F-doped graphene (F_{10}-G) was prepared for comparison (Figures S20–S23), which has the same component as F_x-CNTs but without nanoconfinement effect. Its F content is 0.83 at%, similar to that of F_8-CNTs (0.70 at%). The water contact angle presents insignificant difference between F_{10}-G (138.0°), F_8-CNTs (139.7°), and F_{10}-CNTs (140.4°). The F_{10}-G also shows high efficiency for H_2O_2 electrosynthesis at 0.05 M H_2SO_4, but its FEs_{H2O2} are lower than those of F_8-CNTs and F_{10}-CNTs at 300–500 mA cm^{-2}, and the decrement is more remarkable under higher current

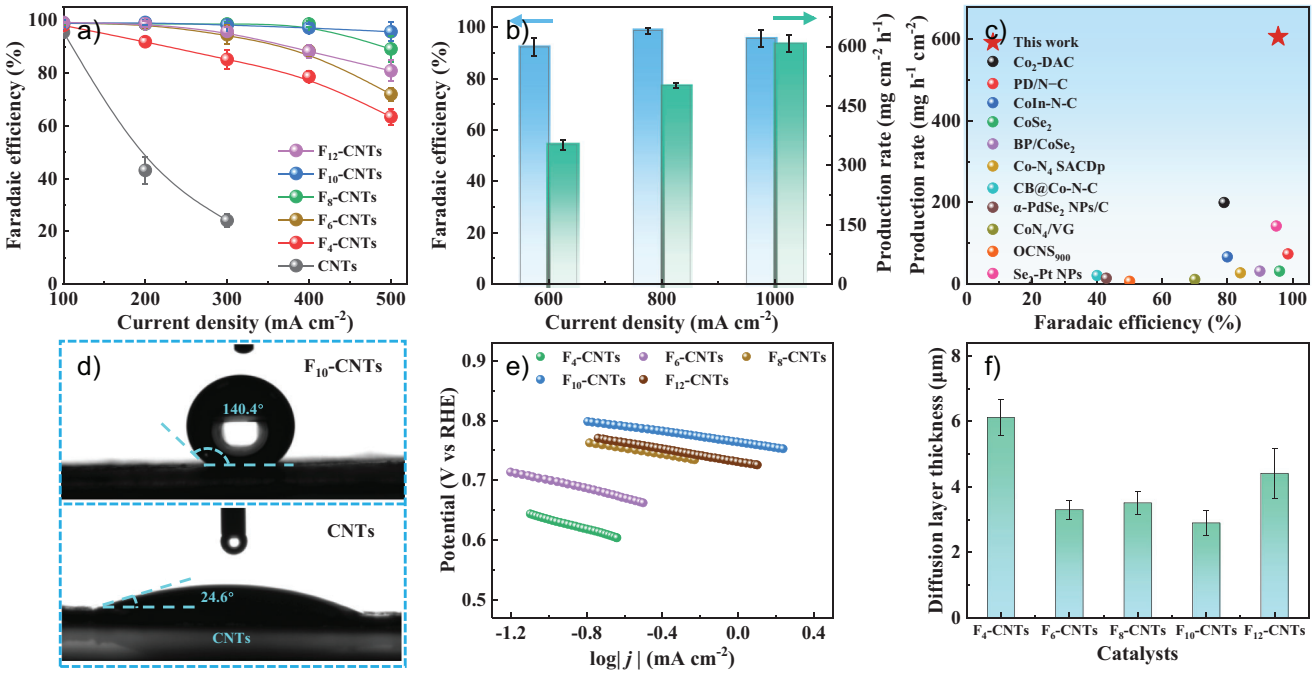

Figure 2. a) FEs_{H2O2} of F_x-CNTs at 100–500 mA cm^{-2} and 0.05 M H_2SO_4. b) FEs_{H2O2} and H_2O_2 yields of F_{10}-CNTs at 600–1000 mA cm^{-2} and 0.05 M H_2SO_4. c) The comparison of FEs_{H2O2} and H_2O_2 production rates between F_{10}-CNTs and reported electrocatalysts in acid (data sources in Table S2). d) Water contact angles of F_{10}-CNTs and CNTs. e) Tafel plots and f) diffusion layer thickness of F_x-CNTs. Error bars represent standard deviation from three independent measurements.

density (Figure 3c). Its corresponding H_2O_2 yields are 1.5–1.6 times lower than those of F_8-CNTs and F_{10}-CNTs (Figure 3d). These results demonstrate that F_8-CNTs and F_{10}-CNTs are superior to F_{10}-G for H_2O_2 electrosynthesis. The calculated diffusion layer thickness of F_{10}-CNTs is 2.9 μm (Figures 3e and S24), slightly smaller than those of F_{10}-G (3.3 μm) and F_8-CNTs (3.5 μm), indicating that F_{10}-G and F_8-CNTs have similar oxygen mass transfer rate and their oxygen mass transfer rates are slower than that of F_{10}-CNTs. The F_{10}-CNTs exhibit smaller Tafel slope than F_{10}-G (58.4 mV dec^{-1}) and F_8-CNTs (55.3 mV dec^{-1}, Figure 3f). Considering that F_8-CNTs and F_{10}-G have similar F content, hydrophobicity, and oxygen mass transfer, the much better performance of F_8-CNTs relative to F_{10}-G may be attributed to the nanoconfinement effect of CNTs. To further explore the nanoconfinement effect, F_8-CNTs were prepared using CNTs with different diameters (As F_{10}-G has the similar F content to F_8-CNTs). The FE_{H2O2} is increased for F_8-CNTs with smaller diameter (Figures 3g and S25), which further confirms that nanoconfinement effect plays a crucial role in enhancing H_2O_2 synthesis.

The local pH values of electrocatalysts during electrocatalysis were measured by in situ technique with an iridium oxide (IrO_x) ring electrode. As shown in Figures 3h and S26, the local pH is rapidly increased for F_{10}-CNTs, F_8-CNTs, F_{10}-G and CNTs@PTFE as the potential is negatively shifted from 0.40 to −0.54 V (versus RHE) in 0.05 M H_2SO_4. Notably, the local pH follows the order of F_{10}-CNTs > F_8-CNTs > F_{10}-G > CNTs@PTFE. It shows the same trend under constant current density (500 mA cm^{-2}, Figure S27). Thus, F-doping is more efficient than PTFE modification for increasing the local pH. Compared with F_{10}-G, F_{10}-CNTs and F_8-CNTs create a more alkaline local environment. In the process of H_2O_2 electrosynthesis, local alkaline environment is favorable for inhibiting the side reaction of hydrogen evolution or H_2O_2 reduction, and improving H_2O_2 selectivity. The phenolphthalein was employed as a chromogenic agent to visualize the surface pH change on F_{10}-CNTs electrode. The color of F_{10}-CNTs surface change from colorless to pink after electrolysis at −0.45 V versus RHE for 20 s in 0.05 M H_2SO_4 (Figure S28 and Video S1). It confirms that a local alkaline environment is formed on F_{10}-CNTs surface during H_2O_2 electrosynthesis. Therefore, both the super hydrophobicity and local pH regulation resulted from F-doping contribute to the enhanced H_2O_2 electrosynthesis on F_{10}-CNTs.

In-situ attenuated total reflection surface-enhanced infrared absorption spectroscopy (ATR-SEIRAS) was used to investigate the *OOH generated on F_{10}-CNTs and F_{10}-G (Figure S29). In O_2 saturated 0.05 M H_2SO_4, a main band at 1224 cm^{-1} and a weak band at 1390 cm^{-1} can be observed (Figure 4a), which are attributed to the O—O stretching vibration of surface adsorbed *OOH and the *OOH bending vibration of adsorbed *HOOH, respectively.[32,33] As the potential is negatively shifted, their peak intensities are increased. The increment on F_{10}-CNTs is more significant than that on F_{10}-G (Figure 4b). These results indicate that F_{10}-CNTs promote $*OOH_{ad}$ generation as compared with F_{10}-G.

DFT calculation was performed to elucidate the effect of F-doping on the intermediate adsorption or reaction energy for oxygen reduction. F-doping can change the structure of

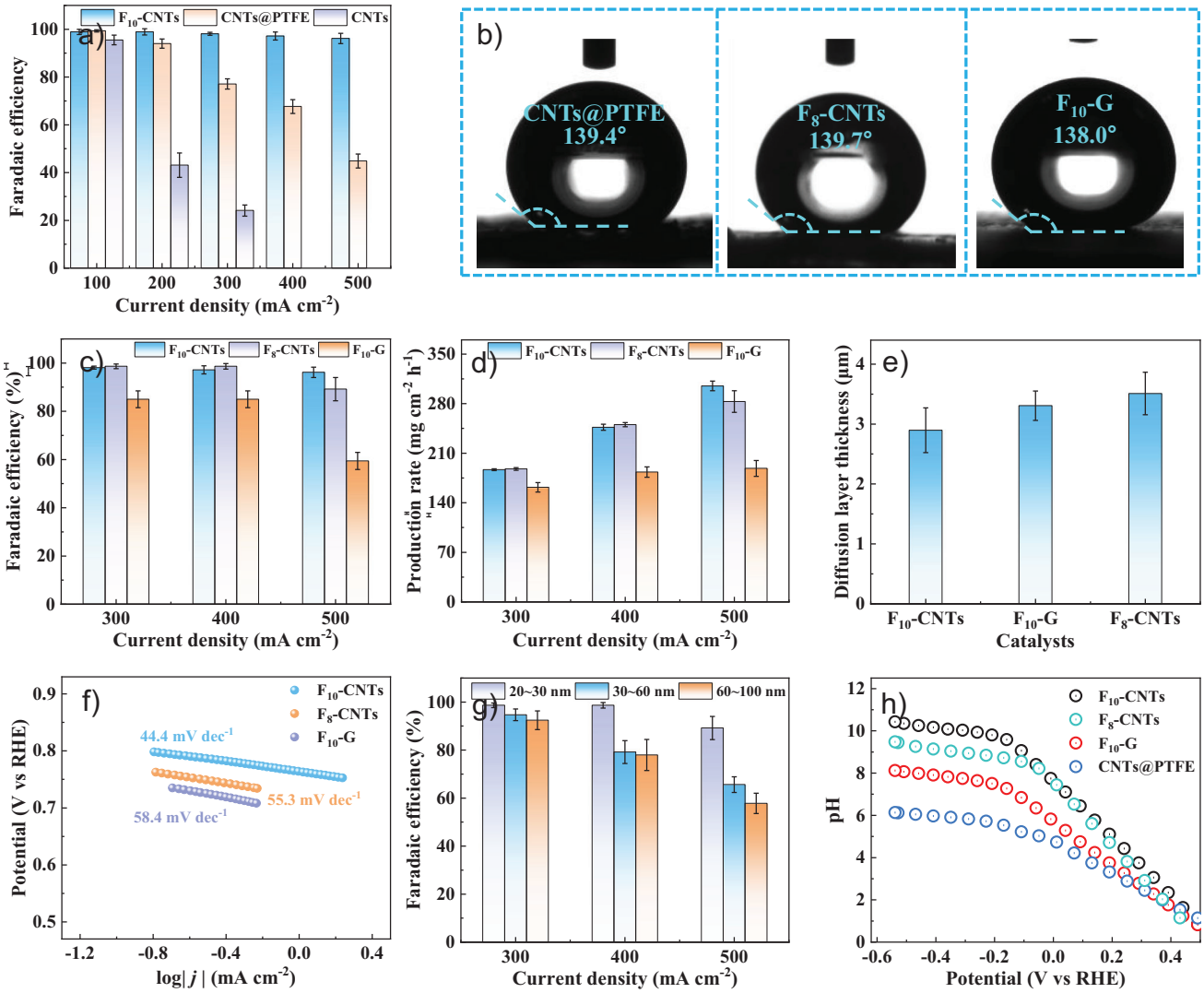

Figure 3. a) FEs_{H2O2} of F_{10}-CNTs, CNTs@PTFE and CNTs. b) Water contact angles of CNTs@PTFE, F_8-CNTs, and F_{10}-G. c) FEs_{H2O2} and d) H_2O_2 yields of F_{10}-CNTs, F_8-CNTs and F_{10}-G at 0.05 M H_2SO_4. e) Diffusion layer thickness and f) Tafel plots for F_{10}-CNTs, F_{10}-G and F_8-CNTs. g) FEs_{H2O2} of F_8-CNTs with different diameters (0.05 M H_2SO_4). h) The local pH values of F_{10}-CNTs, F_{10}-G and CNTs@PTFE in 0.05 M H_2SO_4. Error bars represent standard deviation from three independent measurements.

CNTs (Figure S30), which is consistent with the characterization results. The *OOH generation is an uphill process for H_2O_2 production. The free energy for *OOH generation on F-in-CNTs is only 0.30 eV, which is lower than that on F-out-CNTs (0.40 eV) and and F-G (0.58 eV, Figures 4c and S31). There is obvious electron transfer from active sites to *OOH (Figures S32 and S33), which is conducive to accelerate the 2e⁻-ORR. The inner surface of the confined space can significantly change the interface charge environment,[34,35] which influences the selectivity and kinetics of interactions between F-CNTs and intermediates. These results indicate that the fluorine atoms doped on the internal-surface of CNTs may enhance the nanoconfinement effect of CNTs, resulting in further reduced energy barrier for *OOH generation on F-in-CNTs.

The dynamic behavior of H^+ on the electrode surface has an important effect on the electrochemical reaction (2e⁻-ORR, 4e⁻-ORR or HER). Ab-initio molecular dynamics (AIMD) simulations were executed to analyze the dynamic behavior of H^+ on F-G and F-CNTs surfaces in 0.05 M H_2SO_4 or 0.05 M H_2SO_4/0.01 M K_2SO_4 (potential was −1.0 V). In 0.05 M H_2SO_4, H^+ tends to drift toward the electrode surfaces (Figure 4d). Interestingly, randomly labeled hydrogen ions are more accessible to the surface of F-G than F-CNTs (Figures 4e,f and S34). The dynamic behavior of H^+ on the electrode surfaces results in lower H^+ concentration on the surface of F-CNTs than F-G at the same electrolyte (Figure 4g). It is beneficial to inhibit the side reactions of 4e⁻-ORR or HER during H_2O_2 electrosynthesis. When 0.01 M K_2SO_4 was introduced into the electrolyte, K^+ is more favorable to migrate toward the electrode surface, while H^+ could move away from the F-CNTs and F-G surfaces due to repulsion (Figures 4h, S35, S36 and Video S2). Notably, the performance of F-CNTs were superior to that of

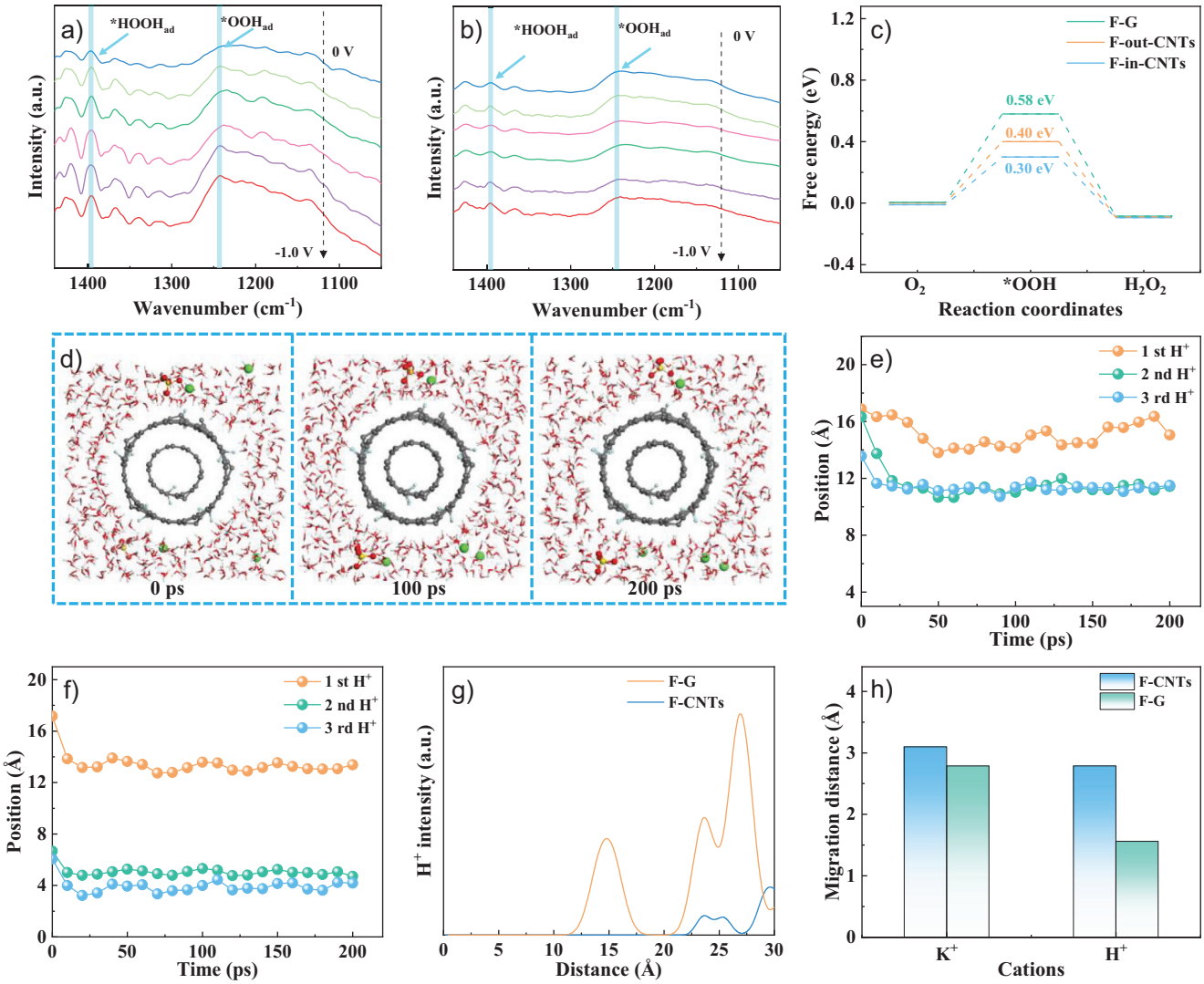

Figure 4. In situ ATR-SEIRAS spectra of a) F_{10}-CNTs and b) F_{10}-G for oxygen reduction at O_2 saturated 0.05 M H_2SO_4. c) Free energy profiles of O_2 reduction at 0.7 V versus RHE. d) Representative periodic modelling for proton distribution on F-CNTs surface at 0.05 M H_2SO_4 under −1.0 V versus RHE (H^+, F atoms, O atoms, S atoms, and H atoms are in green, cyan, red, yellow, and white, respectively). The position evolution (surface normal direction "z") of randomly labeled H^+ on the surfaces of F-CNTs e) and F-G f) in 0.05 M H_2SO_4. H^+ intensities g) and average migration distances h) of H^+ on F-CNTs and F-G surfaces in 0.05 M H_2SO_4.

F-G in both the attraction of K^+ and the repulsion of H^+ (Figures S37–S39). This implies that F-CNTs exhibit more pronounced cationic shielding effects.

Application for H_2O_2 Electrosynthesis in a Wide pH Range

F_{10}-CNTs is selective for acidic H_2O_2 electrosynthesis, and its performance can be further improved with the presence of alkali metal cations (Figure S40). In 0.05 M H_2SO_4/0.01 M K_2SO_4 electrolyte, FEs_{H2O2} are increased to 95.7%–89.8% even at 1.0–1.8 A cm^{-2}. The corresponding H_2O_2 yields are 585.8–814.6 mg cm^{-2} h^{-1} (Figure 5a and Video S3), showing excellent performance for H_2O_2 electrosynthesis. F_{10}-CNTs is also efficient for H_2O_2 electrosynthesis at neutral and alkaline solutions. At 0.1 M Na_2SO_4, its FEs_{H2O2} are 97.1%–89.8% at 500–800 mA cm^{-2} with H_2O_2 yields of 307.8–453.8 mg cm^{-2} h^{-1} (Figure 5b). When the pH is further increased to 13 (0.1 M KOH), the FE_{H2O2} is slightly improved in comparison with neutral and acid conditions, which is 92.0% at 800 mA cm^{-2} (Figure 5c).

The stability of F_{10}-CNTs for H_2O_2 electrosynthesis at industrial-relevant current was examined at 500 mA cm^{-2}. In general, the cell potential almost remains unchanged throughout the 30 h operation in 0.05 M H_2SO_4 (Figure 5d). The concentrations of H_2O_2 produced at 500 mA cm^{-2} are 1677.0–1743.8 mM with FEs_{H2O2} of 89.9%–93.5%, demonstrating the good stability of F_{10}-CNTs electrode for H_2O_2 electrosynthesis at industrial-relevant current density. After the stability test, water contact angle of F_{10}-CNTs electrode is 123.1° (Figure S41a). F_{10}-CNTs is still hydrophobic, although its water contact angle decreases slightly (initial value of

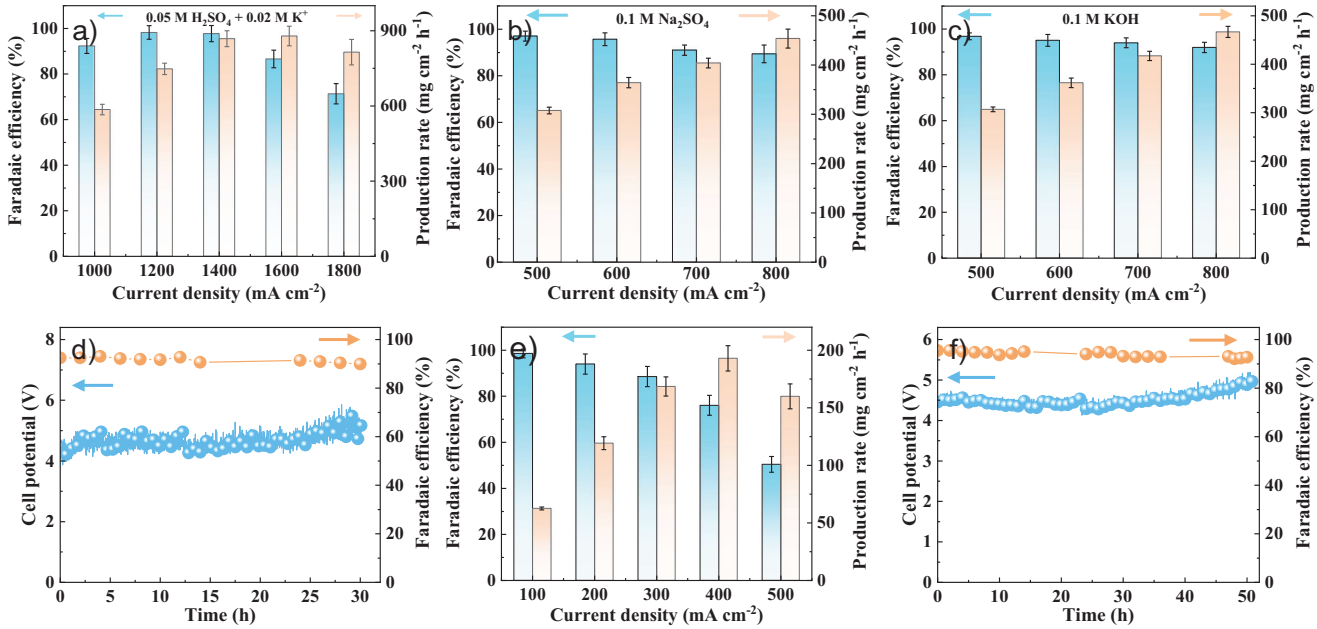

Figure 5. Performance for H_2O_2 electrosynthesis on F_{10}-CNTs in a) 0.05 M H_2SO_4/0.01 M K_2SO_4, b) 0.01 M Na_2SO_4 and c) 0.1 KOH. d) Stability of F_{10}-CNTs for continuous H_2O_2 electrosynthesis at 500 mA cm^{-2}. e) Performance for H_2O_2 electrosynthesis with air supply in 0.05 M H_2SO_4. f) Stability of F_{10}-CNTs for continuous H_2O_2 electrosynthesis under air supply at 200 mA cm^{-2} and 0.05 M H_2SO_4. Error bars represent standard deviation from three independent measurements.

140.4°). In contrast, electrode flooding occurs on CNTs electrode after 9.5 h of operation. TEM images reveal that the microstructures of F10-CNTs and CNTs exhibit no obvious change after stability test (Figures S41b-e). The energy consumption of F_{10}-CNTs for H_2O_2 electrosynthesis is 5.17–7.62 kW h kg_{H2O2}^{-1} at 300–500 mA cm^{-2}, superior than the reported electrocatalyst (Table S3). The applicability of F_{10}-CNTs for H_2O_2 electrosynthesis with air as oxygen source was also evaluated in 0.05 M H_2SO_4. The FE_{H2O2} is higher than 90% at 100–300 mA cm^{-2}, and it declines significantly as the current density increases (Figure 5e), which may be due to limited oxygen supply. Figure 5f shows the stability of H_2O_2 electrosynthesis with air as oxygen source. F_{10}-CNTs is stable for the continuous 50 h of H_2O_2 electrosynthesis with FEs_{H2O2} of 92.1%–95.5% at 200 mA cm^{-2} and 0.05 M H_2SO_4. These results indicate that F_{10}-CNTs is stable for H_2O_2 electrosynthesis at industrial-relevant current.

Conclusion

F-CNTs with F-doped on the inner and outer wall of CNTs were prepared by a simple method. It was efficient for acidic H_2O_2 electrosynthesis with FE_{H2O2} of 99.2%–95.6% and H_2O_2 yields of 351.5–606.6 mg cm^{-2} h^{-1} at industrial-level currents of 600–1000 mA cm^{-2}, outperforming the state-of-the-art catalysts in acidic media. F-doping significantly enhanced the H_2O_2 electrosynthesis performance of CNTs by regulating the electronic structure, enhancing oxygen mass transfer and nanoconfinement effect, which optimize *OOH generation and creates a more alkaline local environment. The F-CNTs demonstrated excellent stability for H_2O_2 electrosynthesis over extended operation. Its pH-universal feature and good performance with air as the oxygen source confirmed its versatility and scalability. These findings provide new insights into catalyst design and local reaction environment regulation for H_2O_2 electrosynthesis. This work highlights the potential of F-CNTs for efficient and sustainable H_2O_2 electrosynthesis.

Acknowledgements

This work was supported by the National Natural Science Foundation of China (22222601 and 22076019) and the Fundamental Research Funds for the Central Universities (DUT23LAB611).

Conflict of Interests

The authors declare no conflict of interest.

Data Availability Statement

The data that support the findings of this study are available from the corresponding author upon reasonable request.

Keywords: F-doped carbon nanotube · Hydrogen peroxide synthesis · Local proton concentration · Nanoconfinement effect · Oxygen reduction

[1] C. Xia, Y. Xia, P. Zhu, L. Fan, H. Wang, *Science* **2019**, *366*, 226–231.
[2] www.gminsights.com/pressrelease/hydrogen-peroxide-market.
[3] B. Lee, H. Shin, A. Rasouli, H. Choubisa, P. Ou, R. Dorakhan, I. Grigioni, G. Lee, E. Shirzadi, R. Miao, J. Wicks, S. Park, H. Lee, J. Zhang, Y. Chen, Z. Chen, D. Sinton, T. Hyeon, Y. Sung, E. Sargent, *Nat. Catal.* **2023**, *6*, 234–243.
[4] S. C. Perry, D. Pangotra, L. Vieira, L. Csepei, V. Sieber, L. Wang, C. Ponce De León, F. C. Walsh, *Nat. Rev. Chem.* **2019**, *3*, 442–458.
[5] W. Fan, Z. Duan, W. Liu, R. Mehmood,J. Qu, Y. Cao, X. Guo, J. Zhong, F. Zhang, *Nat. Commun.* **2023**, *14*, 1426.
[6] K. Lee, J. Lim, M. Lee, K. Ryu, H. Lee, J. Kim, H. Ju, H. Cho, B. Kim, M. Hatzell, J. Kang, S. Lee, *Energy & Environ. Sci.* **2022**, *15*, 2858–2866.
[7] Q. Zhang, X. Tan, N. Bedford, Z. Han, L. Thomsen, S. Smith, R. Amal, X. Lu, *Nat. Commun.* **2020**, *11*, 4181.
[8] H. Kim, M. Ross, N. Kornienko, L. Zhang, J. Guo, P. Yang, B. McCloskey, *Nat. Catal.* **2018**, *1*, 282–290.
[9] W. Peng, J. Qiu, X. Liu, H. Tan, F. Hou, J. Feng, X. Yan, J. Liang, *Adv. Funct. Mater.* **2024**, *34*, 2411353.
[10] J. Xu, X. Zheng, Z. Feng, Z. Lu, Z. Zhang, W. Huang, Y. Li, D. Vuckovic, Y. Li, S. Dai, G. Chen, K. Wang, H. Wang, J. Chen, W. Mitch, Y. Cui, *Nat. Sustain.* **2020**, *4*, 233–241.
[11] H. Sheng, A. Janes, R. Ross, H. Hofstetter, K. Lee, J. Schmidt, S. Jin, *Nat. Catal.* **2022**, *5*, 716–725.
[12] Y. Yang, J. Qin, K. Hu, L. Luo, A. Kumar, D. Zhou, Z. Zhuang, H. Li, X. Sun, *Energy & Environ. Sci.* **2023**, *16*, 491–501.
[13] C. Yang, F. Sun, Z. Qu, X. Li, W. Zhou, J. Gao, *ACS Energy Lett.* **2022**, *7*, 4398–4407.
[14] Z. Lin, Q. Zhang, J. Pan, C. Tsounis, A. Esmailpour, S. Xi, H. Yang, Z. Han, J. Yun, R. Amal, X. Lu, *Energy & Environ. Sci.* **2022**, *15*, 1172–1182.
[15] K. Jiang, J. Zhao, H. Wang, *Adv. Funct. Mater.* **2020**, *30*, 2003321.
[16] B. Ni, P. Shen, G. Zhang, J. Zhao, H. Ding, Y. Ye, Z. Yue, H. Yang, H. Wei, K. Jiang, *J. Am. Chem. Soc.* **2024**, *146*, 11181–11192.
[17] P. Cao, X. Zhao, Y. Liu, H. Zhang, K. Zhao, S. Chen, H. Yu, F. Dong, N. Nichols, J. Chen, X. Quan, *Angew. Chem. Int. Ed.* **2024**, *63*, e202406452.
[18] L. Jing, Q. Tian, X. Li, J. Sun, W. Wang, H. Yang, X. Chai, Q. Hu, C. He, *Adv. Funct. Mater.* **2023**, *33*, 2305795.
[19] Z. Lu, G. Chen, S. Siahrostami, Z. Chen, K. Liu, J. Xie, L. Liao, T. Wu, D. Lin, Y. Liu, T. Jaramillo, J. Nørskov, Y. Cui, *Nat. Catal.* **2018**, *1*, 156–162.
[20] Y. Bu, Y. Wang, G. Han, Y. Zhao, X. Ge, F. Li, Z. Zhang, Q. Zhong, J. Baek, *Adv. Mater.* **2021**, *33*, 2103266.
[21] L. Yu, L. Tang, W. Guo, C. Li, D. Shin, Z. Liu, Y. Lin, *Matter* **2022**, *5*, 1909–1923.
[22] S. Xu, R. Lu, K. Sun, J. Tang, Y. Cen, L. Luo, Z. Wang, S. Tian, X. Sun, *Adv. Sci.* **2022**, *9*, 2201421.
[23] Y. Xia, X. Zhao, C. Xia, Z. Wu, P. Zhu, J. Kim, X. Bai, G. Gao, Y. Hu, J. Zhong, Y. Liu, H. Wang, *Nat. Commun.* **2021**, *12*, 4225.
[24] Y. Long, J. Lin, F. Ye, W. Liu, D. Wang, Q. Cheng, R. Paul, D. Cheng, B. Mao, R. Yan, L. Zhao, D. Liu, F. Liu, C. Hu, *Adv. Mater.* **2023**, *35*, 2303905.
[25] F. Xiang, X. Zhao, J. Yang, N. Li, W. Gong, Y. Liu, A. Burguete-Lopez, Y. Li, X. Niu, A. Fratalocchi, *Adv. Mater.* **2023**, *35*, 2208533.
[26] Y. Liu, L. Li, H. Tan, N. Ye, Y. Gu, S. Zhao, S. Zhang, M. Luo, S. Guo, *J. Am. Chem. Soc.* **2023**, *145*, 19877–19884.
[27] A. Peera, R. Menon, S. Das, A. Alfantazi, K. Karuppasamy, C. Liu, A. Sahu, *Coordin. Chem. Rev* **2024**, *500*, 215491.
[28] J. Park, C. Lee, J. Ju, J. Lee, J. Seol, S. Lee, J. Kim, *Adv. Funct. Mater.* **2021**, *31*, 2101727.
[29] Y. Wen, H. Zhu, J. Hao, S. Lu, W. Zong, F. Lai, P. Ma, W. Dong, T. Liu, M. Du, *Appl. Catal. B-Environ.* **2021**, *292*, 120144.
[30] Y. Liu, T. Sakthivel, F. Hu, Y. Tian, D. Wu, E. Ang, H. Liu, S. Guo, S. Peng, Z. Dai, *Adv. Energy Mater.* **2023**, *13*, 2203797.
[31] J. Xie, X. Zhao, M. Wu, Q. Li, Y. Wang, J. Yao, *Angew. Chem. Int. Ed.* **2018**, *57*, 9640–9644.
[32] C. Tang, L. Chen, H. Li, L. Li, Y. Jiao, Y. Zheng, H. Xu, K. Davey, S. Qiao, *J. Am. Chem. Soc.* **2021**, *143*, 7819–7827.
[33] S. Nayak, I. McPherson, K. Vincent, *Angew. Chem. Int. Ed.* **2018**, *57*, 12855–12858.
[34] J. Xiao, X. Pan, S. Guo, P. Ren, X. Bao, *J. Am. Chem. Soc.* **2015**, *137*, 477–482.
[35] J. Qian, X. Gao, B. Pan, *Environ. Sci. Technol.* **2020**, *54*, 8509–8526.

Manuscript received: February 13, 2025
Revised manuscript received: April 25, 2025
Accepted manuscript online: May 07, 2025
Version of record online: ■■, ■■

Research Article

H_2O_2 Electrosynthesis

G. Zhu, S. Zhao, Y. Yu, X. Fan, K. Liu, X. Quan, Y. Liu* — **e202503626**

Tuning Local Proton Concentration and *OOH Intermediate Generation for Efficient Acidic H_2O_2 Electrosynthesis at Ampere-Level Current Density

Efficient acidic H_2O_2 electrosynthesis was achieved on F-CNTs with Faradaic efficiency of 95.6% at 1.0 A cm^{-2}. F-doping regulated the electronic structure, enhanced nanoconfinement effect and oxygen mass transfer of CNTs, leading to a local alkaline microenvironment and promoted *OOH generation for acidic H_2O_2 electrosynthesis.